PROTEINS: Structure, Function, and Genetics 22:154–167 (1995)

Molecular Dynamics Simulations of Rubredoxin From *Clostridium pasteurianum:* Changes in Structure and Electrostatic Potential During Redox Reactions

Robert B. Yelle, Noh-Sum Park, and Toshiko Ichiye

Department of Biochemistry/Biophysics, Washington State University, Pullman, Washington 99164-4660

ABSTRACT **Molecular dynamics simulations of *Clostridium pasteurianum* rubredoxin in the oxidized and reduced forms have been performed. Good agreement between both forms and crystal data has been obtained (rms deviation of backbone atoms of 1.06 and 1.42 Å, respectively), which was due in part to the use of explicit solvent and counterions. The reduced form exhibits an unexpected structural change: the redox site becomes much more solvent-accessible, so that water enters a channel between the surface and the site, but with little actual structural rearrangement (the rms deviation of backbone atoms between the oxidized and reduced is 0.77 Å). The increase in solvent accessibility is also seen, although to a much lesser extent, between the oxidized and reduced crystal structures of *Pyrococcus furiosus* rubredoxin, but no high resolution crystal or nuclear magnetic resonance solution data exist for reduced *C. pasteurianum* rubredoxin. The electrostatic potential at the iron site and fluctuations in the potential, which contribute to both the redox and electron transfer properties, have also been evaluated for both the oxidized and the reduced simulations. These results show that the backbone plays a significant role (62–70 kcal/mol/e) and the polar side chains contribute relatively little (0–4 kcal/mol/e) to the absolute electrostatic potential at the iron of rubredoxin for both forms. However, both groups contribute significantly to the change in redox state by becoming more polarized and more densely packed around the redox site upon reduction. Furthermore, these results show that the solvent becomes much more polarized in the reduced form than in the oxidized form, even excluding the penetrating water. Finally, the simulation indicates that the contribution of the charged side chains to the electrostatic potential is largely canceled by that of the counterions.** © 1995 Wiley-Liss, Inc.

Key words: iron-sulfur proteins, electron transfer, oxidation-reduction potentials, solvent accessibility

INTRODUCTION

Electron transfer proteins serve a vital function in electron transport, an essential mechanism by which energy flows in all living things. Redox potentials of electron transfer proteins are an important characteristic of these proteins in that their relative values affect the direction and rate of the transfer. Since the redox sites in proteins are at least partially surrounded by the protein itself, the protein microenvironment around the redox site should affect the redox potential. In fact, it has been shown that redox potentials of proteins are considerably different from those of analogs of the protein redox site.[1,2] Furthermore, homologous proteins from different species usually exhibit at least slightly different redox potentials.[3,4] Therefore, it is of interest to study how the microenvironment around the redox site due to the protein matrix should influence the redox potential.

The focus here is on the classical contributions to the redox potential. Several works have established a connection between changes in the classical electrostatic energy upon reduction and the redox potentials.[5–8] Moreover, the electrostatic potential at the redox site is a measure of the polarization of the environment at the site and is thus important to Marcus electron transfer theory, which states that the polarization of the donor and acceptor redox sites fluctuates and that electron transfer can occur when the polarization of the two sites are equal.[9] In addition, while conformational changes can affect the electronic properties of the redox site,[10] the electronic contributions may be calculated separately if they do not affect the rest of the protein. This appears to be a good approximation since the major influence of the quantum mechanical degrees of freedom on the classical degrees is the charge distribution of the redox site, and since the structure of the protein appears to be relatively insensitive to the exact charge distribution.[11] Moreover, the con-

Received May 3, 1994; revision accepted February 9, 1995.

Address reprint requests to Dr. Toshiko Ichiye, Department of Biochemistry/Biophysics, Washington State University, Pullman, WA 99164-4660.

formational fluctuations of the redox site in the simulation are small compared with those contributing to changes in electronic properties of the redox site in ref. 10.

Although several calculations have been done of the oxidized and reduced states of redox-active proteins using Poisson-Boltzmann electrostatics[5] and other non-statistical techniques,[6,7] relatively few molecular dynamics simulations have been done. A simulation of *Clostridium beijerinckii* flavodoxin in water[12] with the flavin mononucleotide (FMN) cofactor in the oxidized and singly reduced semiquinone states had only protein and solvent atoms within a 14-Å sphere around the center of the FMN, i.e., only 51 of the 138 residues freely moving in the simulation, with a shell of 8 Å with positional restraints. Moreover, a detailed comparison was made with the respective crystal structures of the oxidized and reduced flavodoxins, including the structural waters, but little comparison was made of the differences between the oxidized and reduced structures. In another study, the differences in redox potential between the wild-type and a mutant cytochrome c[13] were calculated by the protein dipoles Langevin dipoles (PDLP)[6] method, and by a free energy perturbation method, and were compared with experimental results. However, in this study only two to three water molecules were included explicitly and the other water molecules were modeled as Langevin dipoles, that is, polarizable dipoles fixed on a grid.[6,13]

Here we present the results of molecular dynamics simulations of the iron-sulfur protein rubredoxin (Rd) from *Clostridium pasteurianum* (Cp). Rubredoxins are small proteins (5–20 kDa) with relatively simple redox sites consisting of a single iron tetrahedrally bound to four sulfur atoms from cysteine residues.[14] The main function of rubredoxin is unknown, but it is thought to participate in electron transfer reactions in sulfur-reducing bacteria.[15] A previous study of the changes in structure and electrostatic potential upon reduction in rubredoxin has been done using energy minimization[11]; however, this method neglects thermal fluctuations. It is important to include the contributions of thermal fluctuations, especially in calculating the solvent contribution. Therefore, to study how the microenvironment around the protein influences its electron transfer properties, molecular dynamics simulations of rubredoxin in its oxidized and reduced forms solvated with explicit water with no restraints placed on any atoms have been performed. These were used to assess structural changes upon reduction and to calculate the electrostatic potential and fluctuations in the potential at the redox site.

MATERIALS AND METHODS

The molecular dynamics simulations were carried out using the molecular mechanics package CHARMM 22g2.[16] The simulations were for the systems in the microcanonical ensemble at a temperature of approximately 300 K. The Verlet algorithm was used to propagate the dynamics using a time step of 0.001 ps. The potential energy function combined parameters from CHARMM 19 plus additional parameters for the iron-sulfur site,[11] which have been modified slightly, as given in Table I. A van der Waals repulsion was added to the iron as there is none in the CHARMM 19 parameters and simulations of a redox site analog of Rd in water showed considerable penetration of water into the iron.[17] The value was chosen so that the minimum between Fe^{3+} and a TIP3P water matched that used by Kuharski et al.[18] The energy parameters for the waters were from the TIP3P model.[19] Nonpolar hydrogens were treated via the extended atom model, in which hydrogens are included as part of the heavy atom to which they are attached. All bonds containing hydrogen were held to their equilibrium bond lengths using the SHAKE algorithm.[20] The atom-based force-switch,[21] described briefly below, was used with a switching region between 8.0 and 11.0 Å to approximate the nonbonded forces beyond 8.0 Å. A cutoff distance of 12.0 Å was used for the nonbonded lists and image lists. The nonbonded lists were updated by the heuristic updating procedure, while the image lists were updated every 20 steps. A constant dielectric of one was used throughout the simulation and no atomic polarizability was included, as in previous studies.[11,17]

TABLE I. Fe-S Site Parameters*

Internal coordinates	Oxidized	Reduced	Force constants
Cβ-S	1.84	1.84	450.0
Fe-S	2.267	2.356	80.0
S-S	3.702	3.847	5.758
Cα-Cβ-S	112.5	112.5	50.0
Fe-S-Cβ	101.5	108.2	43.0
S-Fe-S	109.47	109.47	20.0
X-Fe-S-X	0.0	0.0	0.80

*Internal coordinates are in units of Å for bond lengths and degrees for bond angles and dihedral angles. Force constants for bond lengths, bond angles, and dihedral angles are in units of kcal/mol-Å, kcal/mol-deg^2 and kcal/mol-deg^2, respectively.

The coordinates of oxidized Rd from Cp[22,23] were obtained from the Brookhaven Protein Data Bank (5RXN). The protein was first relaxed by 100 steps of steepest descents minimization with oxidized parameters in the presence of its crystal waters. Afterwards, the nearest crystal water to each charged side chain and the two chain termini was replaced by a counterion in order to balance the surface charge of the protein. A sodium ion was placed near each negatively charged side chain (16 total) and the C-terminus and a chloride ion was placed near each positively charged side chain (4 total) and the N-terminus with parameters from CHARMm20 (CHARMm is a registered trademark of Molecular

TABLE II. Lennard-Jones Parameters*

Atom	ε	R_{min}
Fe-O(water)	−0.120	2.84
Na	−0.382	0.95
Cl	−0.240	2.03

*ε, E_{min} (kcal/mole); R_{min} is in Å.

Simulations, Inc.), which are included in Table II. No counterions were placed to balance the charge on the iron-sulfur site because the redox site is more buried than the side chains and is thus less likely to be directly associated with a counterion and because we wanted to compare the oxidized and reduced systems without adding a counterion on reduction. Thus, the system had a net charge of −1 for the oxidized system and −2 for the reduced system and so Ewald sums were not used. The protein was then further solvated by placing it in a pre-equilibrated truncated octahedral shaped box of dimensions 51.0 Å by 44.0 Å by 42.0 Å containing 1,582 TIP3P water molecules. The dimensions were chosen to correspond to the dimensions of Cp Rd in order to provide an even distribution of solvent around the protein. The protein was placed with its center of mass in the center of the box of water and rotated such that its longest dimension corresponded to the x-axis. All water molecules within 2.6 Å of the protein were deleted, resulting in a box containing 1,218 waters and 4,171 atoms total. This structure was used for the initial coordinates for simulations of both the oxidized and reduced forms.

The initial equilibration of the oxidized Rd entailed 5.0 ps of Gaussian assignment of velocities every 0.2 ps to solvent only (protein and counterions fixed), followed by 5.0 ps of assigning velocities to the solvent and counterions, and then 10.0 ps of assigning velocities to the whole system. The velocities were allowed to scale every 0.2 ps if the temperature was less than 290 K or greater than 300 K for 5 ps (but did not actually scale), and were followed by 50 ps of dynamics in which the system was not perturbed. Data were collected every 0.01 ps for the last 50.0 ps, during which the average temperature was 297.1 ± 3.6 K.

For the simulation of the reduced Rd, the initial equilibration of assigning velocities was the same as for the oxidized simulation. Velocities were scaled as above for 4.8 ps and then the system was allowed to evolve unperturbed for another 5.2 ps. Data were collected every 0.01 ps for the last 70 ps, during which the average temperature was 299.6 ± 3.9 K. During the first 15–20 ps of the collection phase a water molecule penetrated into the redox site. The last 50 ps of collection after water penetration was used for analysis.

The choice of the atom-based force-switch method[21] and the addition of counterions were motivated by several test calculations that used the more conventional energy-switch[16] with switching regions of either between 8 and 10 Å or between 7.5 and 11.5 Å and no counterions. The energy-switch function[16] gives a large, artificial force in the switching region for Coulombic interactions that significantly affects the dynamics of the system. The atom-based force-switch method applies a switching function to the forces rather than the potential, thus eliminating the artificial peak in the force in the switching region that occurs with the energy-switch.[21] In four previous attempts at simulating the rubredoxin in the reduced form using the energy-switch, all showed the highly charged loop region (residues 17–24) moving away from the rest of the protein with the best structure having a backbone root mean-square (rms) deviation of 2.4 Å from the crystal structure. The energy-switched simulation of the oxidized form was more stable than the energy-switched simulations of the reduced form, but even it had a backbone rms deviation of 1.34 Å from the crystal structure of oxidized Cp Rd. Other test simulations used a switched group-shift method that shifts the potential energy between charge-charge interactions between groups of atoms with a net charge by a constant before applying the switching function and otherwise switches the potential energy when at least one of the interacting groups is net neutral.[21] These resulted in backbone rms deviations for the oxidized and reduced forms (with counterions) of 1.25 and 1.79 Å, respectively, from the crystal structure and deviations from each other of 1.43 Å, with most of the deviation again due to the movement of the loop, although less so than with the energy-switched simulations. The counterions were added to increase protein stability, screen the charged side chains, and give a rough estimate of their effect on the electrostatic potential.

RESULTS

Structure of Rubredoxin

Structural properties of Rd in the dynamics simulations are discussed in this section, beginning with the overall differences followed by specific structural features. Comparisons with crystal results are given to assess reliability of the simulations, in addition to descriptions of structural changes upon reduction.

The average structures for oxidized and reduced Rd from the dynamics trajectories are first compared with the crystal structure. No structure for reduced Cp Rd is available, so a comparison was made with the oxidized structure. The average oxidized structure was in very good agreement with the oxidized crystal structure, the protein backbone (henceforth, all references to backbone refer to N, Cα, and C atoms) having an overall rms deviation of 1.06 Å. The largest rms deviations for backbone atoms between the average oxidized structure and the crystal structure occur near the iron-sulfur site (Pro 40 and Val 8), at residues 34–36, at both chain termini, and at the loop region consisting of residues 17–24 (Fig. 1).

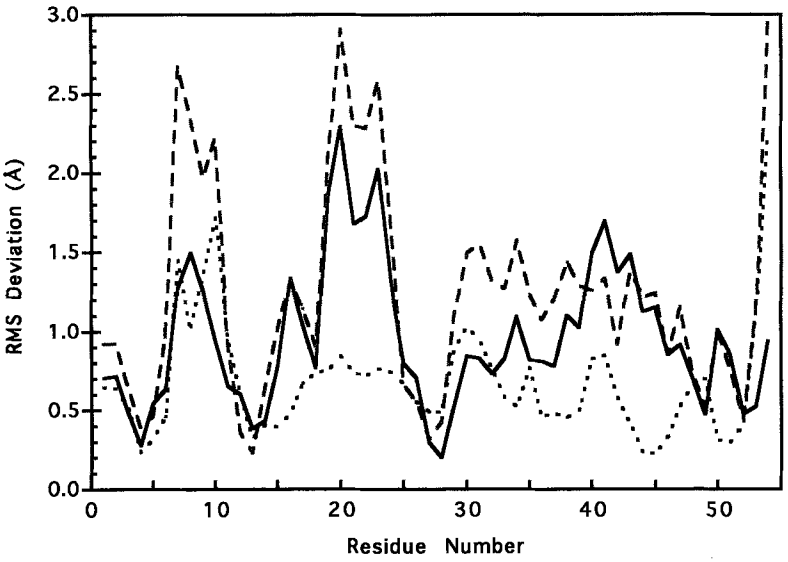

Fig. 1. The rms deviation per residue between the backbones of the crystal structure and the average oxidized structure (solid line), between the backbones of the crystal structure and the average reduced structure (dashed line), and between the average oxidized structure and average reduced structure (dotted line).

The differences in structure are somewhat larger between the reduced and crystal structure than between the oxidized and crystal structure, with an overall backbone rms deviation of 1.42 Å, the largest differences occurring near the redox site (7–10, 40–42), the loop region (20–24), and the C-terminal region (Fig. 1). The overall backbone rms deviation between the oxidized and reduced structures is 0.77 Å. From the backbone rms deviation per residue between the average reduced and average oxidized structures (Fig. 1), the largest difference is at residue 10 near the redox site. The next largest changes are at the C-terminus, residues 29–31, and near the other cysteines of the redox site at residues 7–11, 40 and 41, the latter being the site of the greatest changes in earlier minimization studies.[11] The average radius of gyration (R_G) was 10.33 Å for the oxidized form, and 10.28 for the reduced form compared with 10.1 Å for the crystal structure.

The extent of the protein motions seen in the simulations was assessed by calculating the rms fluctuations of atomic positions in the dynamics trajectory and comparing them with the B-factors from X-ray experiments. A large contribution to the values of B-factors can be attributed to the motions of the atoms in the crystal[24] and are related to the rms fluctuations, $\langle \Delta r^2 \rangle$ by

$$B = \frac{8\pi^2 \langle \Delta r^2 \rangle}{3}.$$

The rms fluctuations were plotted versus residue for backbone atoms from the crystal B-factors and from both dynamics trajectories (Fig. 2). Overall, the fluctuations from both simulations are featureless, as are the crystal results, and have a somewhat lower background value, with the major differences being the greatly increased motion of the N- and C-termini in the crystal. One notable area is the peak at the loop region 20–23 in the oxidized simulation that is seen (to a lesser extent) in the reduced simulation. This is the region that exhibited large movements in the reduced but not oxidized forms in the preliminary simulations with other types of cutoffs. Also, there are large fluctuations in the reduced simulation at residues 7–10.

The internal structure of the iron-sulfur site was examined in detail since the structural variation may affect the quantum mechanical degrees of freedom of the redox site.[10] The bond lengths of the average oxidized structure and the crystal structure are in good agreement, i.e., within 0.07 Å, and those from the reduced simulation reflect the differences in the parameters (Table I). Most bond angles for the oxidized and reduced structures are quite close to the crystal (within 8.0°). However, there are two notable changes in the dihedral angles that occurred during the equilibration phase of both simulations. These changes resulted in differences between the average structures and the crystal of about 50° in the Cα9-Cβ9-Sγ9-Fe angle in the oxidized and about 180° in the reduced, and about 80° in the Cβ9-Sγ9-Fe-Sγ39 dihedral angle in the oxidized and about 90° in the reduced. No dihedral angles change conformation during the collection run in either the oxidized or reduced simulation. With the exception of the above two dihedral angles, the rest are in good agreement with the crystal values.

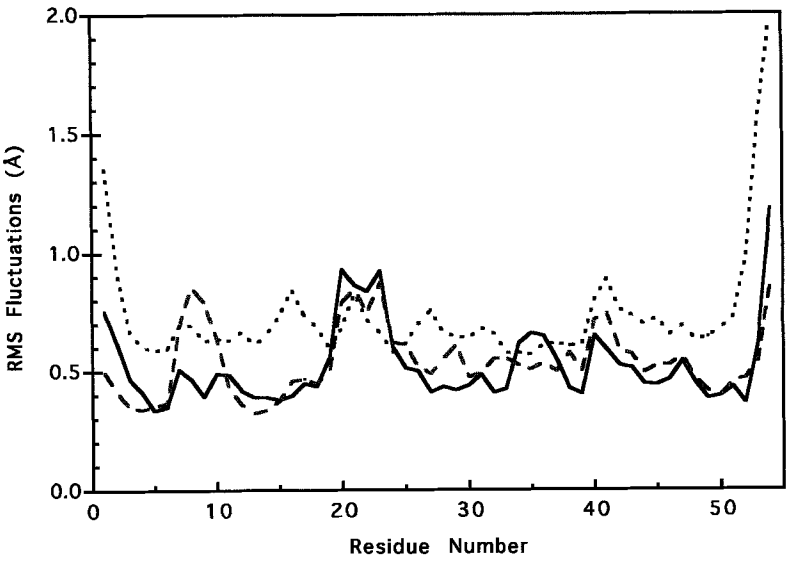

Fig. 2. The rms fluctuations of backbone atoms from crystal B-factors (dotted line), the simulation of the oxidized form (solid line), and the simulation of the reduced form (dashed line).

Since it has been suggested that hydrogen bonding interactions in the redox sites in iron-sulfur proteins may be determinants of protein redox potential,[25–28] all potential hydrogen bonds between the amide backbone and redox site were investigated. In both simulations, the hydrogen bond angles tend to deviate from ideality more than in the crystal structure. Most of the donor-acceptor distances were within 0.8 Å of the crystal values, while most of the hydrogen-acceptor distances were within 0.7 Å of the crystal values. The major differences between the oxidized simulation and the crystal structure were the N10-Sγ9 and N11-Sγ9 hydrogen bonds, whose donor-acceptor and hydrogen-acceptor distances deviated by more than 1.0 Å, and resulted in a net decrease of about 4.4 kcal/mole/e to the electrostatic potential at the Fe. There are a few large changes in hydrogen bond distance upon reduction, the largest differences being 2.2 Å for N11-Sγ9 and 1.9 Å for N10-Sγ9, and these changes have a 1.1 kcal/mole/e and 3.7 kcal/mole/e affect on the electrostatic potential at the Fe, respectively. These changes in hydrogen bond distance may also affect the electrostatic potential at the sulfurs and, if close enough, the ionization potential of the redox site.

Another structural property, the radial distribution functions, g(r), of all polar and charged groups around the iron, was also calculated, since the locations of different types of atoms with respect to the iron determine the electrostatic potential. From the functions for the amide N, the carbonyl O, and the water O (Fig. 3), and the amide H and Cα, the carbonyl C, and the water H (not shown), it is evident that the dipole moments of the protein backbone and the water are pointed with the positive end toward the negatively charged redox center, as may be expected. (Similar plots are shown in Yang et al.[17]) More interesting changes can be seen in the rearrangement of the atoms nearest the iron upon reduction (distances here are given from the iron). For instance, the amide N g(r) for the oxidized form shows peaks at 3.8, 5.0, and 5.7 Å, with areas of 2, 4, and 6 N, respectively, whereas the reduced form shows peaks at 3.5, 4.3, 5.0, and 5.7 Å, with areas of 1, 2, 5, and 4 N, respectively, showing a net shift of 2 N within 5.5 Å upon reduction. The second, more dramatic, change is the increase in number of waters near the iron upon reduction. In the oxidized form there are on average only one water molecule (at −5.3 Å) within 6 Å of the iron, the approximate nearest distance to the surface from the iron, and five within 7 Å of the iron. However, in the reduced form, there are one water at 2.2 and two at 4.1 Å, and there are on average four molecules within 6 Å of the iron and eight within 7 Å. The mechanism for the water penetration appears to be the 1.5-Å movement of the backbone at Val 8 (Fig. 4). In the CpRd crystal structure, the closest water is 7.1 Å away, and there are only two within 8 Å. Moreover, no increase in the number of water molecules near the iron is observed between the oxidized and reduced *Pyrococcus furiosus* (PfRd) crystal structures, although a slight increase has been noted in crystal structures of other redox proteins (E. Adman, personal communication). On the other hand, it appears there is room for more than the crystal waters since during the equilibration in which only the solvent and the counterions moved around the fixed protein, the number of waters within 6 Å of the iron is one in the oxidized simulation and four in the reduced simulation.

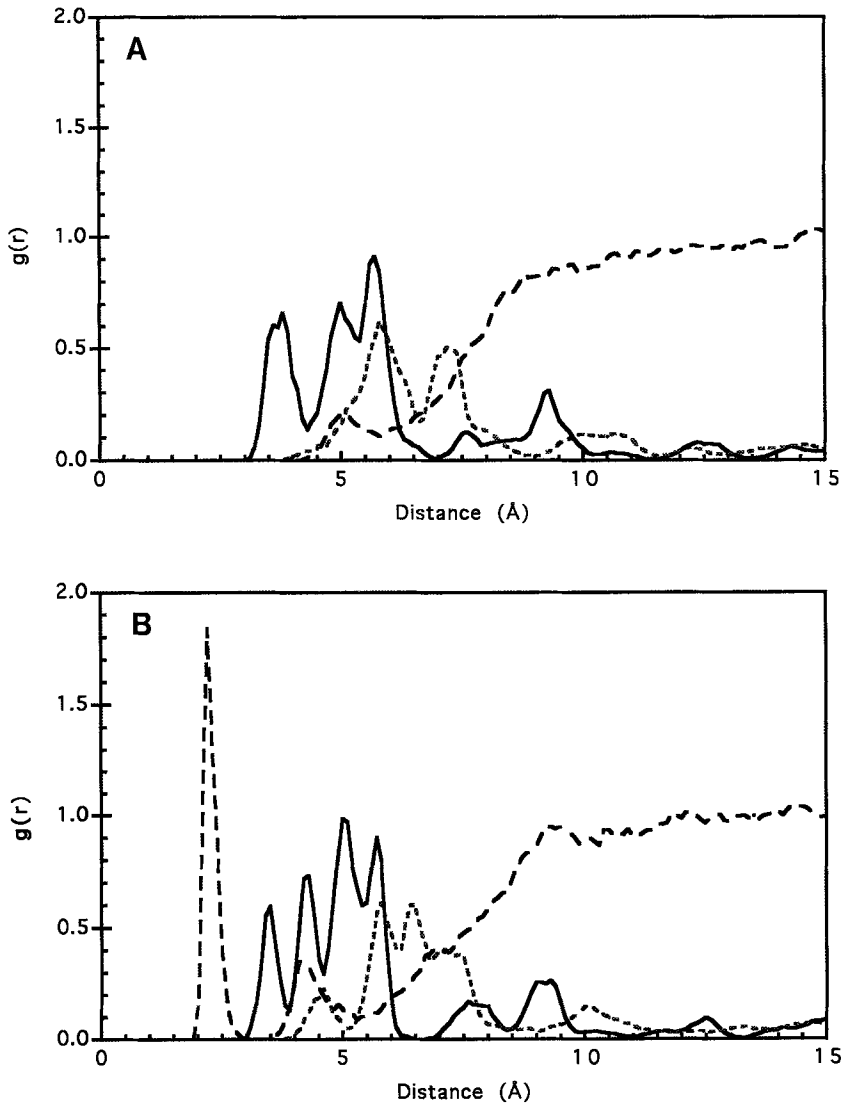

Fig. 3. Radial distribution functions of various atoms around the iron in the oxidized form (**A**) and the reduced form (**B**): amide nitrogens, g_{FeN} (solid line), carbonyl oxygens, g_{FeO} (short dashed line), and water oxygens, g_{FeOw} (long dashed line).

To further investigate the water penetration, the solvent-accessible areas of redox site atoms are compared for the crystal structure of CpRd, the oxidized and reduced simulation structures, the crystal structures of PfRd in the oxidized and reduced forms,[30] and the average nuclear magnetic resonance (NMR) structure of PfRd,[31] which presumably mimics the reduced PfRd (Table III). (PfRd has one less N-terminal residue and so consensus numbering based on CpRd will be used for both.) In all of the structures, the iron is completely inaccessible to solvent. The solvent-accessible area in the average oxidized structure is actually less than that of the crystal structure, but there is a notable increase in solvent-accessible area in the average reduced structure, mostly at Cβ9 and Cβ42. A small increase in solvent accessibility is observed in the crystal structures of Pf in the reduced form compared with the oxidized form,[30] again at Cβ42. In addition, the NMR structure of the Zn-substituted PfRd shows only a slight increase in solvent accessibility of Cβ42, compared with the oxidized crystal, but with a net decrease of the entire redox site.

Finally, the distributions of counterions in the simulations were also examined. The distribution of counterions is not fully equilibrated since it would take about 100 ns for an ion to circumnavigate the protein only one time, using a diffusion rate of 0.1–0.2 $Å^2$/ps, the value for Na^+ and Cl^- in aqueous solution. This estimate is an upper limit, since the

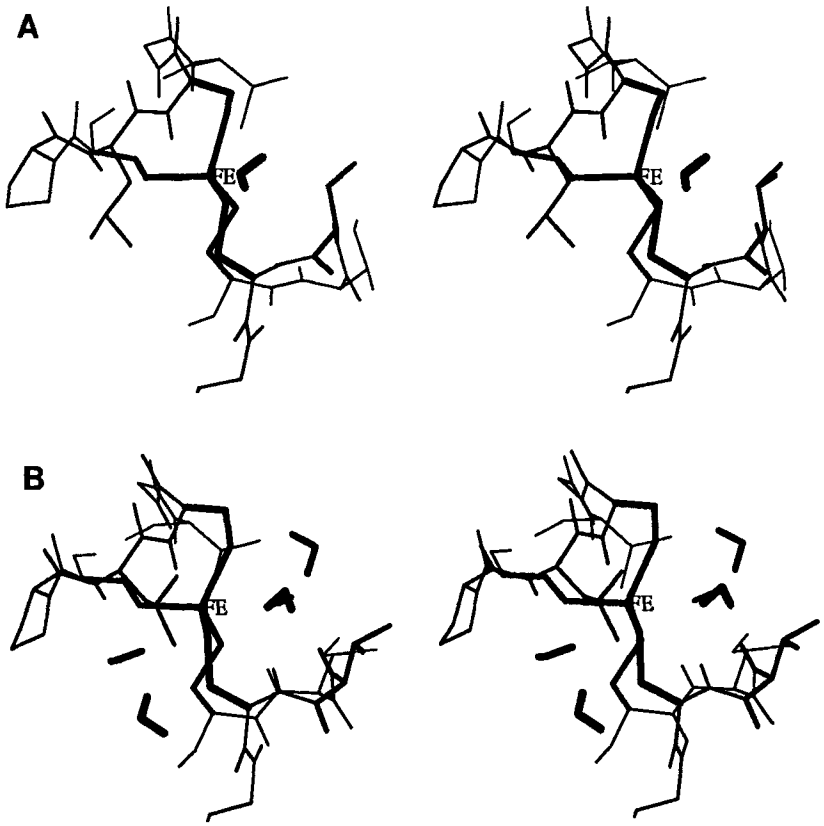

Fig. 4. A frame from the simulation of the oxidized form (**A**) and the reduced form (**B**), showing the redox site and waters within 6 Å of the iron. Note the difference in structure of the Val 8 side chain between the two simulations. (Picture generated using the program MOLSCRIPT.[29])

rate near a protein would be slower. However, the counterions appear to have reached a fairly stable position with respect to the protein in that their mean-square displacements from their charged side chain partners are fairly constant during the collection run, and their contribution to the electrostatic potential appears to be stable, as judged from their contribution versus time (not shown). In general, about half of the counterions in both simulations preferred not to be in close contact with charged side chains. In the oxidized simulation, only 9 of 17 sodium ions and 3 of 5 chloride ions remained ion paired, defined as being less than 5.0 Å away from an oppositely charged side chain. The average initial distance from a counterion to a charged group on the protein was 3.6 Å, but the average distance during the 50 ps of the production run was 4.5 Å. In the reduced simulation, the counterions had the same initial positions as in the oxidized form but drifted even more from their ion-pairs than in the oxidized form, giving an average distance of 6.0 Å with 9 of the 17 sodium ions; only one chloride ion remaining ion-paired.

Electrostatic Environment Around the Iron

The electrostatic environment around the iron was examined in this section via the electrostatic potential at the iron, which can be calculated from the radial distribution function by

$$\Phi(R) = 4\pi \int_0^R r^2 \sum_{i \neq \text{FeS}} g_{\text{Fe}-i}(r) \frac{Z_i \rho_i}{r} dr$$

or more directly from the simulations by

$$\Phi(R) = \left\langle \sum_{\substack{i \neq \text{FeS} \\ r_i < R}} \frac{Z_i}{r_i(t)} \right\rangle$$

at $R = \infty$, where the sum over i is over all atoms except Fe, S, and C of the redox site (FeS), r_i is the distance of atom i from the iron, Z_i is the charge of atom i, ρ_i is the average density of atom i, and $\langle \cdots \rangle$ denotes a time-average. The latter equation was used in the results presented here. By evaluating the above to finite values of R, the contribution of only atoms within a distance R of the iron to Φ can

TABLE III. Solvent Accessibility (Å^2) of Iron-Sulfur Site in Cp and Pf Rubredoxin

Atom	Cp Crystal	Average Ox	Average Red
Sγ6	0.0	0.0	0.7
Cβ6	0.0	0.0	0.0
Sγ9	0.0	3.2	0.0
Cβ9	3.5	0.8	4.5
Sγ39	0.2	0.0	0.0
Cβ39	0.0	0.0	0.0
Sγ42	0.0	0.0	0.0
Cβ42	20.0	13.6	20.9
Total	23.7	17.6	26.1
Atom	Ox Pf Crystal	Red Pf Crystal	Pf NMR
Sγ6	0.1	0.0	0.0
Cβ6	0.0	0.0	0.0
Sγ9	0.0	0.0	0.0
Cβ9	14.4	13.8	13.0
Sγ39	0.0	0.0	0.0
Cβ39	0.0	0.0	0.0
Sγ42	0.2	0.0	0.0
Cβ42	15.4	18.1	16.7
Total	30.0	31.9	29.7

be evaluated. A dielectric constant of 1.0 was used and no cutoffs were used for these calculations.

The contributions of various groups of atoms to the total electrostatic potential (i.e. $R = \infty$ value) at the iron (Table IV) show that the backbone makes a large contributions (62 kcal/mole/e) in the oxidized form, with relatively no contribution by the polar side chains. The contributions of the charged side chains is also very large, but is essentially negated by the counterions. The contributions of various groups of atoms (defined as sets of atoms with integral charge using CHARMM parameters) to the electrostatic potential at the Fe for all atoms within a given distance from the iron are given in Figure 5. It is important to recognize that these figures do not show the value of the electrostatic potential at a given distance from Fe but rather the contributions of all atoms within a given radius R of the Fe to the electrostatic potential at the Fe. For the oxidized form, within the first 10 Å, the peptide backbone makes the largest contribution to the electrostatic potential, although it levels off after 7 Å. The solvent does not make a significant contribution until about 9 Å and reaches a maximum at 19 Å but levels off or decreases after 19 Å. Apparently, waters further from the redox site are being oriented by interactions with images from the periodic boundary conditions, although it may be caused by the solvent oriented by the abundant negatively charged side chains. Upon reduction, the relative contributions of each group are fairly similar to the oxidized simulations, with the most remarkable difference being the increase in the solvent contribution. This is due to a drastic increase in the number of water molecules [from one to four within 6 Å of the iron (Fig. 3), as mentioned earlier] near the site and to polarization of these waters. The penetrating water described earlier contributes about 35 kcal/mole/e to the electrostatic potential, although, even without this water, the solvent contribution is still quite high for the reduced form (69.1 kcal/mole/e). Both the backbone and polar side chains become more polarized (in general, we do not make a distinction between increase in potential due to increased population versus orientation, and we refer to both as polarization) upon reduction. The charged side chain contribution actually decreases upon reduction, but the charged side chains are mostly outside the cutoffs of the electrostatic forces. In fact, it can be easily seen that the major contributions by charged side chains, backbone termini, and counterions are outside the cutoffs (Fig. 5). The contribution of the counterions did not change as drastically with time as expected, starting with a net potential of 276.2 kcal/mole/e at the initial placement of counterions (i.e., before equilibration) and having average values of 266.8 and 268.6 kcal/mole/e during the collection runs of the oxidized and reduced simulations, respectively.

The fluctuations in the electrostatic potential were also calculated as a function of distance for the different polar and charged groups. As can be seen in Figure 6A, for the oxidized form the charged side chains and counterions can contribute large fluctuations in the electrostatic potential. However, these contributions cancel one another, as indicated by the total fluctuations in Table IV. The peptide backbone makes the largest contributions to the fluctuations in the potential within the first 6 Å of the iron. Although the solvent does not make an appreciable contribution to the potential until after 9 Å, the fluctuations in the potential due to the waters are significant before then. The fluctuations in electrostatic potential for the reduced form are greater in general than for the oxidized form. The large peak at 2 Å in the solvent is due to the penetrating water molecule. The reason for the large magnitude of the fluctuations in potential at this distance is that small changes in position and orientation at close distances correspond to large changes in potential. Excluding the penetrating water at 2.2 Å, the fluctuations in the potential are changed by about 3 kcal/mole, which makes it approximately equal to the fluctuations for the oxidized form.

DISCUSSION

This section focuses on two points: the relevance of structural changes observed upon reduction and the factors contributing to the observed redox potentials.

Simulation and crystallographic structures of oxidized CpRd are in good agreement (1.06 Å rms deviation of backbone atoms). The major change in the

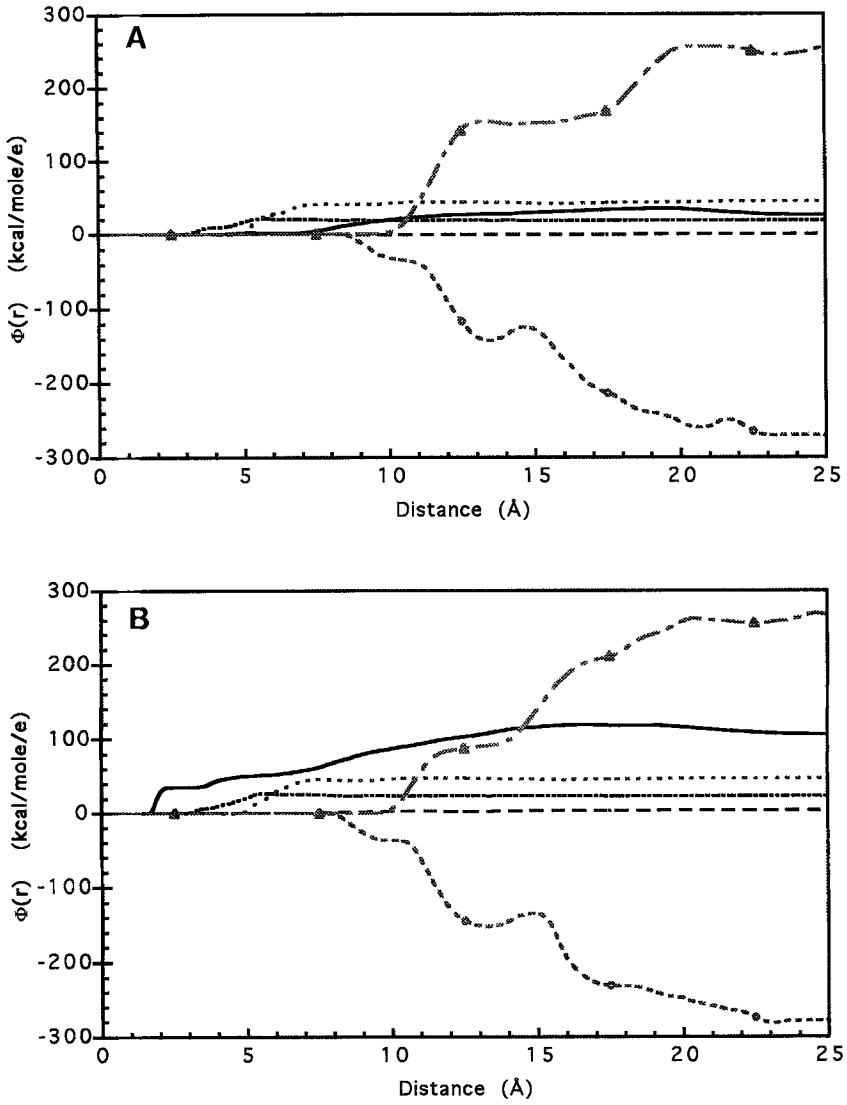

Fig. 5. Contributions to the electrostatic potential at the iron versus distance from the iron for all groups in the oxidized form (**A**) and the reduced form (**B**). Backbone amide group (short dashed line), backbone carbonyl group (medium dashed line), polar side chains (long dashed line), solvent (solid line), charged side chains (dotted line with circles), and counterions (dot-dashes with triangles).

simulation structure of CpRd upon reduction is the increased amount of solvent penetrating the redox site due to a small rearrangement of the backbone near Val 8. Apparently, the increase in charge magnitude of the redox site from -1 to -2 upon reduction attracts water into the redox site area. Of the 13 Rds whose sequences are known,[30] Val 8 is conserved in 9 of them and is replaced by another hydrophobic residue, either Ile or Leu, in the others. Experimental studies of the redox properties of mutations of Val 8 to the smaller Ala or the larger Ile or Leu would be of interest to see how solvent accessibility of the redox site influences the electron transfer properties.

Unfortunately, there is a high resolution crystal structure only for the oxidized form of CpRd, although there are crystal structures for the oxidized and reduced forms of PfRd,[30] as well as an NMR structure of a Zn-substituted PfRd,[31] which presumably mimics the reduced PfRd. One might expect Rds from different bacteria to have similar structures in the reduced form (in addition to the oxidized) if Rds function as electron transfer proteins. However, the degree of structural change upon reduction in the simulation (0.77-Å rms deviation of backbone atoms) is somewhat larger than is predicted by crystal data for PfRd (backbone rms deviation of 0.25 Å)[30] or other proteins.[12,32] Also, neither water penetration nor the Val 8 movement upon reduction in the simulation is observed in ei-

TABLE IV. Contributions of Various Groups to the Electrostatic Potential at the Iron (kcal/mol/e) for Oxidized and Reduced CpRd, Calculated From the Simulation*

	Oxidized form		Reduced form	
Group type	Electrostatic potential	rms fluctuations in potential	Electrostatic potential	rms fluctuations in potential
BB	61.6	4.8	70.0	4.2
PSC	−0.4	1.2	3.7	0.8
CG	−269.8	4.6	−278.5	4.1
CI	266.8	4.7	268.6	4.3
SOLV	24.8	9.8	104.4 (69.1)	12.3 (9.2)
BB + PSC	61.2	5.2	73.7	4.2
BB + PSC + SOLV	86.0	9.3	178.2 (142.9)	12.3 (9.5)
BB + PSC + CG + CI	55.1	7.6	63.9	6.1
CG + CI	−3.0	4.4	−9.9	4.6
Total	82.3	7.7	168.3 (133.0)	11.6 (8.7)

*BB, backbone; PSC, polar side chains; SOLV, solvent; CG, charged groups (side chains + chain termini); CI, counter-ions. The numbers in parentheses are the potentials and fluctuations excluding the penetrating water in the reduced form.

ther the reduced crystal of PfRd or the Zn-substituted PfRd. On the other hand, the reduced PfRd crystal structure is obtained from a crystal that is crystallized in the oxidized state and then reduced so that crystal forces may prevent large changes. Moreover, PfRd is a hyperthermophilic bacteria, and preliminary simulations of reduced PfRd at 298 K indicate no penetration of water. Since the NMR studies were done at 45°C[31] and the crystal data were collected at −160°C (D. Rees, personal communication), it is possible that the structural changes occur at the high temperatures normal for the bacteria. Furthermore, a transition in the temperature dependence of redox potential of PfRd as the temperature is raised from 25°C to 80°C[33] indicates some sort of structural change, possibly an increased flexibility of the protein, thereby allowing solvent penetration. If one assumes then that the flexibility of the hyperthermophilic PfRd at high temperatures resembles the flexibility of the mesophilic CpRd at room temperature, we would predict that water penetration may occur in reduced CpRd in solution at room temperature but only at higher temperatures for reduced PfRd. Moreover, although the distance of 2.2 Å for the closest approach of the water may be dependent on the parameterization of the iron-sulfur site, the motion of the backbone near Val 8 allowing the entry is slight so the penetration by water seems likely, although perhaps not as close as 2.2 Å. Simulations of PfRd at high temperatures are in progress.

The most compelling experimental arguments for water penetration come from other proteins. For instance, very recent NMR studies of oxidized and reduced horse heart cytochrome c[34] show an increase in the number of water molecules near the redox site in the higher charge states of the site upon reduction. In particular, one water, which has been argued to be catalytically important based on the crystal structures,[32] moves from 5.6 Å in the reduced form to 9.3 Å in the oxidized form accompanied by the movement of a nonpolar residue (in this case an isoleucine) as in Rd. Although the water in the simulation of the reduced form of CpRd is much closer to the Fe (2.2 Å) than in the cytochrome c study, this is easy to understand in that the tetrahedral coordination of the Fe in the redox site of Rd is much more open than the octahedral coordination of the heme Fe in cytochrome c, thus allowing closer approach of the water, as has been seen in simulations of an analog in water.[17] As in our Rd results, the water is closer in the more highly charged state of the redox site, since the net charge of the heme can be calculated via

$$\text{protoheme}^{2-} + \text{Fe}^{2+/3+} \rightarrow \text{heme}^{1-/2-} + 2\text{H}^{+}.$$

The net charge on the protoheme is −2 because of the two proprionic groups. However, the catalytically active water is found at about 5.6 Å in both the oxidized and reduced crystal structures. Since the cytochrome c was originally crystallized in the reduced form and then oxidized, the water may be trapped at the shorter distance of the reduced form. This would be consistent with our explanation of why no close water is seen in the reduced PfRd, since it was crystallized originally in the oxidized state, and so the water may be "trapped" outside.

Further experimental evidence for water penetration in other systems comes from proton exchange studies on ferredoxins and HiPIPs.[27] For HiPIPs, the redox site is buried and there is no proton exchange near the metal center unless the protein is partially unfolded. However, for ferredoxins (Fd), proton exchange is observed near the metal center, and the extent of proton exchange depends on the oxidation state of the protein. These results suggest that the metal center in Fd is accessible to aqueous

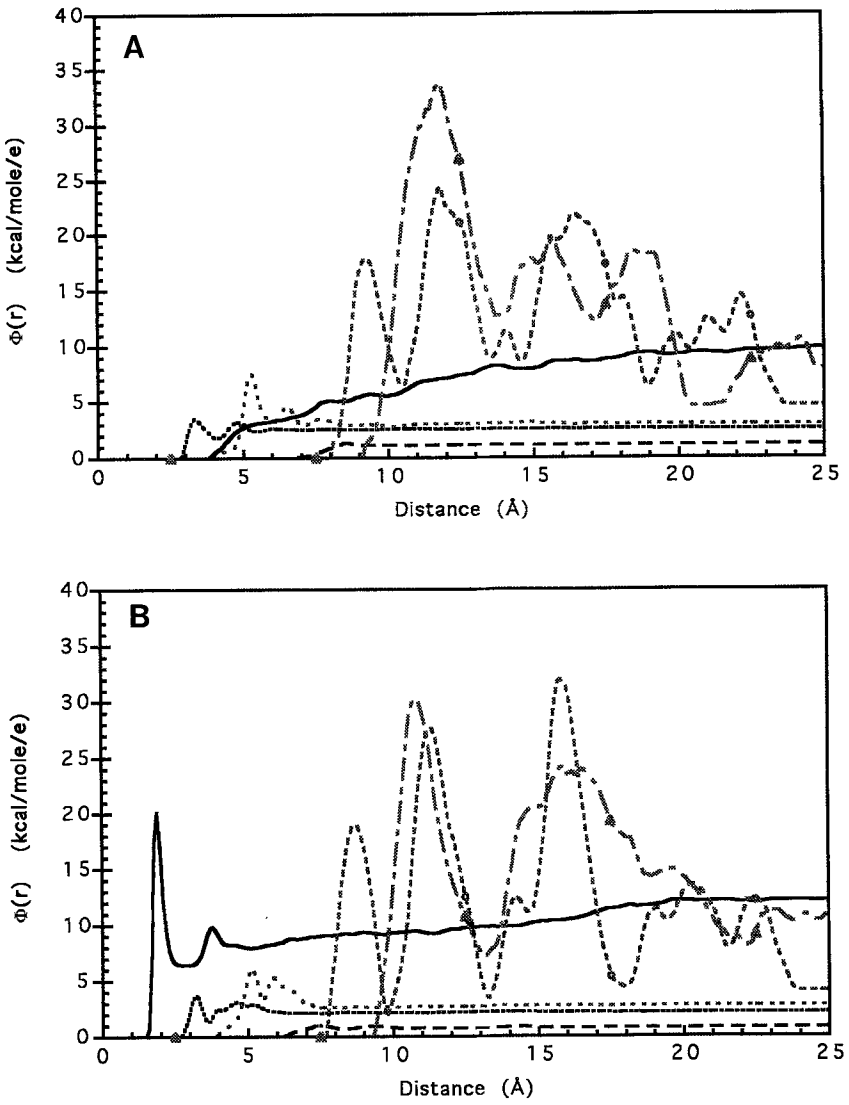

Fig. 6. Contributions to the fluctuations in electrostatic potential at the iron versus distance from the iron for all groups in the oxidized form (**A**) and the reduced form (**B**). Key as in Figure 5.

solvent and that this solvent accessibility is dependent on the oxidation state.

Finally, crystal structures of flavodoxin show that redox active oxygen of the FMN is strongly hydrogen bonded in the reduced state (net charge −1) to a water molecule (W-3 in the semiquinone crystal structure[35]) contrary to the oxidized structure (net charge 0).[36] This was also seen in the molecular dynamics simulation.[12] The backbone rms of the oxidized and the semiquinone crystal structure is 0.28 Å, while that of the oxidized and fully reduced simulation structures is 0.63 Å.

The observed changes upon reduction in the simulation can also be compared with those seen in an earlier energy minimization study.[11] The changes seen in the simulation are of greater magnitude (overall backbone rms 0.77 Å) than seen in the minimization studies, since the latter gave as little as 0.14–0.26 Å rms change. The greater degree of change in the simulation is not surprising since thermal fluctuations should allow the structure to cross more energy barriers and thus deviate more. The structural changes near the redox site are of comparable magnitude between the molecular dynamics and minimization studies, although water penetration is not seen and the resulting change in electrostatic potential due to the protein backbone is similar.[37]

To see if the observed water penetration upon reduction is an artifact of the simulation, several different simulations were performed. As mentioned in the Methods section, several preliminary calcula-

tions with and without counterions using different types of switching functions and cutoffs were done, all of which showed water penetration upon reduction. Since α-helices are much less stable in simulations with periodic boundary conditions that do not use Ewald sums versus those that do use them[38] and since no Ewald sums were used here, simulations of reduced CpRd using a spherical shell of water with no special boundary conditions were performed (with both the switch group-shift and the atom force-switch), but they also show water penetration (R.B. Yelle and T. Ichiye, unpublished results). Also, it is possible that the electrostatic interactions in the real protein are reduced due to atomic polarizability, which is not included explicitly here. However, simulations of polarizable models of water indicate that atomic polarizability contributes little to the structure of most systems (D. Smith, personal communication). Thus, proper parameterization of the partial charges can implicitly include atomic polarizability.

An interesting aside is that in our earlier simulations, the loop region 17–24 moved away from the rest of the protein upon reduction, more so without counterions or when periodic boundary conditions were not used and less so with the addition of counterions and the switch group-shift energy function. The general sensitivity to these conditions indicates that the real protein may be only marginally stable. CpRd has 16 negatively charged and 4 positively charged side chains (Rds are in general highly negatively charged proteins) and only one apparent salt bridge between Asp 35 and Lys 46. There are also no disulfide bonds, so the protein backbone is held together by hydrogen bonds and van der Waals interactions and the iron-sulfur site. In particular, there are only two hydrogen bonds between the loop and the rest of the protein.

The other aspect of Rd studied here is the contribution of different types of atoms to the electrostatic potential of Rds. Of the protein atoms, the charged side chains make the largest contribution to the electrostatic potential. However, of the four Rds that have been shown to have high structural similarity by crystallography and that have measured redox potentials, there is a range of net surface charge between −6 and −12 and yet there is little variation in redox potential.[8] The simulations here support this since the charged side chain contributions are essentially canceled by the counterions. It is also interesting to note that the fluctuations in electrostatic potential due to the side chains are in large part canceled by those due to the counterions, indicating that the side chains and the counterions are correlated in their motion. Of course, the extent to which the charged side chain contributions are canceled depends not only on the distribution of counterions but on the concentration of counterions used. Overall, these results indicate that the ionic strength should affect redox potential, which agrees with experimental results showing that ionic strength can have a significant effect on the redox potential and electron transfer rates of some reactants.[39–41] Although the ionic concentrations (0.18 M Cl^- and 0.6 M Na^+) used here are quite high, the local ionic strength of a protein in excess salt may be expected to be high. Better simulation treatments of counterions are of obvious importance, although the effect of the counterion migration on the electrostatic potential at the iron is much smaller than expected in both simulations.

Other factors contributing to the electrostatic potential include the distribution, orientation, and strength of polar groups. The polar groups considered here are the peptide backbone (treated as two groups separately, the amide group and carbonyl group), the polar side chains, and the solvent. The peptide backbone is the most polarized of the protein groups studied and makes the largest net contribution to the electrostatic potential, since the charged side chains are mostly counterbalanced by counterions. The contribution of the polar side chains is small in both simulations, as well as in the crystal structures of four Rds whose redox potentials have been measured and whose backbones show a high degree of structural similarity.[8] Since the overall differences in the experimental redox potentials is small, it appears that small variations in the backbone near the redox site may contribute to the observed differences in redox potentials. The electrostatic potential results for the polar groups of the protein are similar to earlier energy minimization results.[37] Moreover, although water is excluded from the redox site in the oxidized form, it still makes an appreciable contribution to the electrostatic potential and is significantly increased in the reduced form, due to the increased population and polarization of solvent near the redox site, especially inside 6 Å. This suggests an important role of the solvent in affecting the redox properties of the redox site.

Generally, the low dielectric environment of the protein is probably the most important reason why the redox potentials of Rds are different from analogs of the redox site. Perhaps a primary role for the protein is the exclusion of water from the redox site since the less polar groups in the protein, combined with its rigidity, allows less polarization around the redox site than seen in simulations of a redox site analog in water.[17] However, the degree of penetration of the solvent into the redox site also plays a role and is important for explaining the experimental redox potential for the Holm-Ibers analog in dimethylformamide.[17]

Overall, the possibility of large structural changes upon reduction and the concomitant changes in electrostatic potential at the iron may at first seem to be unreasonable if in fact Rds are involved in electron transfer, although this function for Rd has been ques-

tioned by Adams.[33] However, the actual change in the protein, i.e., the movement of Val 8 to increase solvent accessibility, is slight. This change causes a large change in potential upon reduction for the isolated molecule, which would make it less likely for the molecule to be oxidized unless it is bound to its donor molecule. This is because the donor binding close to the redox site could prevent Val 8 from moving, thus preventing water from penetrating the redox site of the protein, which would result in the lowering of its redox potential and of the activation energy for transfer to the acceptor. This type of change in redox potential has been observed in the methylamine dehydrogenase-amicyanin-cytochrome c551i complex in methylamine metabolism, but no structural mechanism has been verified.[42] Thus, the changes observed here would be relevant to redox potential measurements of free Rd but not of Rd complexed with its biologically relevant partner.

CONCLUSIONS

The structural changes upon reduction in CpRd have been examined via molecular dynamics simulations of the oxidized and reduced forms. The simulated oxidized and reduced structures are in good agreement with the oxidized crystal structure (rms 1.06 and 1.42 Å, respectively). The good agreement was achieved by use of the explicit water and counterions, and the atom-based force-switch method for nonbonded interactions, which gave better results than the group energy-switch. The rms deviation between the simulated oxidized and reduced structures is 0.77 Å. The major change upon reduction is the increased amount of solvent penetrating the protein at the redox site due to movement of a valine residue, which was simply a small rearrangement of the peptide backbone and is due to an increase in the magnitude of the charge of the redox site from -1 to -2.

The penetration of water upon reduction in the simulations is important for several reasons. First, if it is a real phenomenon, it has important implications for the redox properties of Rd and so it should be looked for experimentally. Second, if it is not found experimentally, current simulation techniques of proteins in water must be reevaluated as the same results were obtained under different conditions. Rubredoxin is an important test case as it is a highly charged protein with no disulfides and few salt bridges. Third, if it is found experimentally, the necessity for explicit models of water in simulations becomes apparent as the water penetration cannot be modeled in a continuum model. Finally, these results indicate that careful analysis of the structure of proteins in simulation should be made since the rms deviation of the protein from the oxidized crystal increases from 1.06 Å for the oxidized to only 1.42 Å for the reduced, and yet the implications for electrostatic potential and thus the function of this protein are enormous.

We have also studied the classical contributions of various groups to the electrostatic potential at the iron. Our results indicate that the electrostatic potential due to explicit counterions essentially completely negates the contribution of the charged side chains in the protein. Moreover, the fluctuations in the potentials of the counterions and charged side chains appear to be highly anti-correlated. There is a substantial increase in total electrostatic potential upon reduction due to the increased number and polarization of polar groups around the redox site, almost exclusively due to the solvent and protein polar groups.

ACKNOWLEDGMENTS

We thank Elinor Adman, David Smith, and Doug Rees for helpful discussions. This work was supported by grants from the National Institutes of Health (1R29 GM45303-01A1) and the National Science Foundation (MCB-9118085), and by funds from Washington State University. We also acknowledge the VADMS center at Washington State University.

REFERENCES

1. Lane, R.W., Ibers, J.A., Frankel, R.B., Papaefthymiou, G.C., Holm, R.H. Synthetic analogues of the active sites of iron-sulfur proteins. 14. Synthesis, properties, and structures of bis(*o*-xylyl-α-α′-dithiolato)ferrate(II,III) anions, analogues of oxidized and reduced rubredoxin sites. J. Am. Chem. Soc. 99:84–98, 1977.
2. Harbury, H.A., Cronin, J.R., Fanger, M.W., Hettinger, T.P., Murphy, A.J., Myer, Y.P., Vinogradov, S.N. Complex formation between methionine and a heme peptide from cytochrome c. Proc. Natl. Acad. Sci. U.S.A. 54:1658–1664, 1965.
3. Meyer, T.E., Przysiecki, C.T., Watkins, J.A., Bhattacharyya, A., Simondsen, R.P., Cusanovich, M.A., Tollin, G. Correlation between rate constant for reduction and redox potential as a basis for systematic investigation of reaction mechanisms of electron transfer proteins. Proc. Natl. Acad. Sci. U.S.A. 80:6740–6744, 1983.
4. Moura, I., Moura, J.J.G., Santos, M.H., Xavier, A.V., and Le Gall, J. Redox studies on rubredoxins from sulphate and sulphur reducing bacteria. FEBS Lett. 107:419–421, 1979.
5. Gunner, M.R., Honig, B. Electrostatic control of midpoint potentials in the cytochrome subunit of the *Rhodopseudomonas viridis* reaction center. Proc. Natl. Acad. Sci. U.S.A. 88:9151–9155, 1991.
6. Churg, A.K., Warshel, A. Control of the redox potential of cytochrome c and microscopic dielectric effects in proteins. Biochemistry 25:1675–1681, 1986.
7. Langen, R., Jensen, G.M., Jacob, U., Stephens, P.J., Warshel, A. Protein control of iron-sulfur cluster redox potentials. J. Biol. Chem. 267:25625–25627, 1992.
8. Swartz, P.D., Beck, B.W., Ichiye, T. J. Biol. Chem., submitted.
9. Marcus, R.A., Sutin, N. Electron transfers in chemistry and biology. Biochim. Biophys. Acta 811:265–322, 1985.
10. Loew, G.H., Chadwick, M., Steinberg, D.A. Calculated properties of the active site complex of oxidized rubredoxins I. Electron distribution and electronic energies as a function of conformation. Theor. Chim. Acta. 33:125–136, 1974.
11. Shenoy, V., Ichiye, T. Influence of protein flexibility on the redox potential of rubredoxin: Energy minimization studies. Proteins 17:152–160, 1993.
12. Leenders, R., van Gunsteren, W.F., Berendsen, H.J.C., Visser, A.J.W.G. Molecular dynamics simulations of oxidized and reduced *Clostridium beijerinckii* flavodoxin. Biophys. J. 66:634–645, 1994.
13. Langen, R., Brayer, G.D., Berghuis, A.M., McLendon, G.,

Sherman, F., Warshel, A. Effect of Asn52 → Ile mutation on the redox potential of yeast cytochrome c: Theory and experiment. J. Mol. Biol. 224:589–600, 1992.
14. Eaton, W.A., Lovenberg, W. The iron-sulfur complex in rubredoxin. In: "Iron-Sulfur Proteins." Vol. II. Lovenberg, W., ed. New York: Academic Press, 1973:131–162.
15. Le Gall, J., Moura, J.J.G., Peck, H.D., Jr., Xavier, A.V. Hydrogenase and other iron-sulfur proteins from sulfate-reducing and methane-forming bacteria. In: "Iron-Sulfur Proteins." Spiro, T.G., ed. New York: John Wiley & Sons, 1982:177–248.
16. Brooks, B.R., Bruccoleri, R.E., Olafson, B.D., States, D.J., Swaminathan, S., Karplus, M. CHARMM: A program for macromolecular energy, minimization, and dynamics calculations. J. Comp. Chem. 23:327–341, 1983.
17. Yang Y., Beck, B.W., Ichiye, T. Aqueous solvation of a rubredoxin redox site analog: A molecular dynamics simulation. J. Am. Chem. Soc. 115:7439–7444, 1993.
18. Kuharski, R.A., Bader, J.S., Chandler, D., Sprik, M., Klein, M.L., Impey, R.W. Molecular model for aqueous ferrous-ferric electron transfer. J. Chem. Phys. 89:3248–3257, 1988.
19. Jorgensen, W.L. Transferable intermolecular potential functions for water, alcohols, and ethers. Application to liquid water. J. Am. Chem. Soc. 103:335–340, 1981.
20. Rychaert, J.P., Ciccotti, G., Berendsen, H.J.C. Numberical integration of the cartesian equation of motion of a system with constraints: Molecular dynamics of *n*-alkanes. J. Comput. Phys. 23:327–341, 1977.
21. Steinbach, P.J., Brooks, B.R. New spherical-cutoff methods for long-range forces in macromolecular simulations. J. Comp. Chem. 15:667–683, 1994.
22. Watenpaugh, K.D., Sieker, L.C., Jensen, L.H. The structure of rubredoxin at 1.2 Å resolution. J. Mol. Biol. 131: 509–522, 1979.
23. Watenpaugh, K.D., Sieker, L.C., Jensen, L.H. Crystallographic refinement of rubredoxin at 1.2 Å resolution. J. Mol. Biol. 138:615–633, 1980.
24. Petsko, G., Ringe, D. Fluctuations in protein structure from x-ray diffraction. Annu. Rev. Biophys. Bioeng. 13: 331–371, 1984.
25. Adman, E., Watenpaugh, K.D., Jensen, L.H. NH···S hydrogen bonds in *Peptococcus aerogenes* ferredoxin, *Clostridium pasteurianum* rubredoxin, and *Chromatium* high potential iron protein. Proc. Natl. Acad. Sci. U.S.A. 72:4854–4858, 1975.
26. Carter, C.W., Jr. New stereochemical analogies between iron-sulfur electron transport proteins. J. Biol. Chem. 252: 7802–7811, 1977.
27. Backes, G., Mino, Y., Loehr, T.M., Meyer, T.E., Cusanovich, M.A., Sweeney, W.V., Adman, E.T., Sanders-Loehr, J. The environment of Fe_4S_4 clusters in ferrodoxins and high-potential iron proteins. New information from x-ray crystallography and resonance Raman spectroscopy. J. Am. Chem. Soc. 113:2055–2064, 1991.
28. Blake, P.R., Park, J.B., Adams, M.W.W., Summers, M.F. Novel observation of NH···S(Cys) hydrogen-bond-mediated scalar coupling in ^{113}Cd-substituted rubredoxin from *Pyrococcus furiosus*. J. Am. Chem. Soc. 114:4931–4933, 1992.
29. Kraulis, P.J. MOLSCRIPT: A program to produce both detailed and schematic plots of protein structures. J. Appl. Crystallogr. 24:946–950, 1991.
30. Day, M.W., Hsu, B.T., Joshua-Tor, L., Park, J.-B., Zhou, Z.H., Adams, M.W.W., Rees, D.C. X-ray crystal structures of the marine hyperthermophilic archaebacterium *Pyrococcus furiosus*. Protein Sci. 1:1494–1507, 1992.
31. Blake, P.R., Park, J.-B., Zhou, Z.H., Hare, D.R., Adams, M.W.W., Summers, M.F. Solution-state structure by NMR of zinc-substituted rubredoxin from the marine hyperthermophilic archaebacterium *Pyrococcus furiosus*. Protein Sci. 1:1508–1521, 1992.
32. Takano, T., Dickerson, R.E. Redox conformational changes in refined tuna cytochrome c. Proc. Natl. Acad. Sci. U.S.A. 77:6371–6375, 1980.
33. Adams, M.W.W. Novel iron-sulfur centers in metalloenzymes and redox proteins from extremely thermophilic bacteria. Adv. Inorg. Chem. 38:341–396, 1992.
34. Qi, P.X., Urbauer, J.L., Fuentes, E.J., Leopold, M.F., Wand, A.J. Structural water in oxidized and reduced horse heart cytochrome c. Structural Biol. 1:378–382, 1994.
35. Smith, W.W., Burnett, R.M., Darling, G.D., Ludwig, M.L. Structure of the semiquinone form of flavodoxin from *Clostridium MP*. J. Mol. Biol. 117:195–225, 1977.
36. Burnett, R.M., Darling, G.D., Kendall, D.S., LeQuesne, M.E., Mayhew, S.G., Smith, W.W., Ludwig, M.L. The structure of the oxidized form of clostridial flavodoxin at 1.9 Å resolution. J. Biol. Chem. 249:4383–4392, 1974.
37. Shenoy, V. Contribution of protein environment to redox potentials of rubredoxin and cytochrome c. M.S. Thesis. Washington State University, 1992.
38. Schreiber, H., Steinhauser, O. Cutoff size does strongly influence molecular dynamics results on solvated polypeptides. Biochemistry 31:5856–5860, 1992.
39. Christensen, H.E.M., Conrad, L.S., Ulstrup, J. Redox potential and electrostatic effects in competitive inhibition of dual-path electron transfer reactions of spinach plastocyanin. Arch. Biochem. Biophys. 301:385–390, 1993.
40. Goldkorn, T., Schejter, A. Electrostatic effects on the kinetics of oxidation-reduction reactions of c-type cytochromes. J. Biol. Chem. 254:12562–12566, 1979.
41. Reid, L.S., Mauk, M.R., Mauk, A.G. Role of heme proprionate groups in cytochrome b_5 electron transfer. J. Am. Chem. Soc. 106:2182–2185, 1984.
42. Gray, K.A., Davidson, V.L., Knaff, D.B. Complex formation between methylamine dehydrogenase and amicyanin from *Paracoccus denitrificans*. J. Biol. Chem. 263:13987–13990, 1988.